Bone 94 (2017) 42–49

Contents lists available at ScienceDirect

Bone

journal homepage: www.elsevier.com/locate/bone

Full Length Article

Microscale mechanical and mineral heterogeneity of human cortical bone governs osteoclast activity☆

K. Pernelle [a,b], L. Imbert [a,c], C. Bosser [a], J-C. Auregan [a,d], M. Cruel [a], A. Ogier [a], P. Jurdic [b], T. Hoc [a,*]

[a] LTDS UMR CNRS 5513, Ecole Centrale Lyon, 36 avenue Guy de Collongue, 69134 Ecully, France
[b] Institut de Génomique Fonctionnelle de Lyon UMR5242, Université de Lyon, CNRS, Ecole Normale Supérieure de Lyon, 46, allée d'Italie, 69364 Lyon cedex 07, France
[c] Mineralized Tissues Laboratory, Hospital for Special Surgery, New York, NY, United States
[d] Département de l'Orthopédie pédiatrique, Necker—Hopital des enfants Malades, AP-HP, Paris Descartes, 145 rue de Sèvres, 75014 Paris, France

ARTICLE INFO

Article history:
Received 27 May 2016
Revised 22 September 2016
Accepted 6 October 2016
Available online 08 October 2016

Keywords:
Osteoclasts
Biomechanics
Matrix mineralization
Nano indentation
Raman spectroscopy

ABSTRACT

Human cortical bone permanently remodels itself resulting in a haversian microstructure with heterogeneous mechanical and mineral properties. Remodeling is carried out by a subtle equilibrium between bone formation by osteoblasts and bone degradation by osteoclasts. The mechanisms regulating osteoclast activity were studied using easy access supports whose homogeneous microstructures differ from human bone microstructure. In the current study, we show that human osteoclasts resorb human cortical bone non-randomly with respect to this specific human bone microstructural heterogeneity. The characterization of this new resorption profile demonstrates that osteoclasts preferentially resorb particular osteons that have weak mechanical properties and mineral contents and that contain small hydroxyapatite crystals with a high carbonate content. Therefore, the influence of human bone microstructure heterogeneity on osteoclast activity could be a key parameter for osteoclast behaviour, for both *in vitro* and clinical studies.

1. Introduction

Bone remodeling occurs throughout life and provides the bone turnover required to adapt both structure and architecture of bone tissue to its mechanical environment. Harmonious remodeling is vital to maintain the biological and mechanical characteristics of healthy bone [1–3]. Osteoclasts - cells of a hematopoietic origin - are one of the three main bone cell types that play a crucial role in the bone remodeling cycle [4]. Mature bone-resorbing osteoclasts adhere tightly to the bone surface at the sealing zone and dissolve both the inorganic and organic components of the bone matrix by secreting protons and enzymes [5]. This resorption phase initializes bone remodeling and thus determines the bone areas that will be substituted. Impaired osteoclast activity is involved in many bone diseases, such as osteoporosis [6] and osteogenesis imperfecta [7]. Thus, osteoclasts are prime targets in the development of new therapeutic treatments [8]. Moreover, resorption is an essential parameter in the formulation of better performing biomaterials whose bioresorbability has to be controlled [9]. Recent studies on osteoclasts have allowed for a better understanding of the mechanisms involved in the differentiation of these cells and the intracellular mechanisms that are responsible for the resorption, the regulation of the resorption process remains unclear. Particularly, the behaviour of osteoclasts and their capacity to function in a cyclic manner - alternating between resorption and migration phases - has not been fully elucidated. In this study, we postulated that the *in vitro* observations of these alternating resorption and migration phases are regulated by the microstructure of the support used. The resorption profile was observed, for the first time, on human cortical bone in which the heterogeneous microstructure differs from the supports that are routinely used to investigate osteoclasts *in vitro*.

Previous *in vitro* studies on resorption were carried out using substrates that were either synthetic or natural - such as bovine bone or dentin. However, the osteoclast behaviour (adhesion, activity) varies according to the nature of the substrates [10,11]. For synthetic substrates, the osteoclastic activity varies according to the composition, roughness, and size of the hydroxyapatite crystals [11]. Regarding natural substrates, each has its own composition and microstructure; although their composition is similar, dentin has a tubular structure [12], whereas bovine bone is plexiform. Under the same culture conditions, the surface area of dentin resorbed by osteoclasts is 11 times larger with 7 times more pits per square centimetre than bovine bone [10]. Thus, the characteristics and organization of the material microstructures predispose them to be more or less resorbed. This observation suggests that the intracellular function of osteoclasts is modulated by the support (adhesion capacity – enzyme efficiency).

☆ Competing financial interests: The authors declare no competing financial interests.

* Corresponding author at: 36 avenue Guy de Collongue, 69134 Ecully, France.
E-mail address: thierry.hoc@ec-lyon.fr (T. Hoc).

http://dx.doi.org/10.1016/j.bone.2016.10.002
8756-3282/

Human cortical bone has a specific heterogeneous haversian microstructure composed of osteons [13] that are formed from adjacent concentric lamellae of type 1 collagen sprinkled with hydroxyapatite crystals and are delimited at their periphery by cement lines [14,15]. The microstructural heterogeneity is observed for mechanical [16] and mineral properties between osteons and interstitial bone. Although the microstructure of human cortical bone is different from other species [17] or other substrates that are usually used to study osteoclast behaviour, the only previous study investigating the resorption of human bone is from 1986. Using techniques available at the time and a mixture of chick osteoclasts, it was reported that resorption by such osteoclasts was confined at 60% to a single mineral density phase [18]. In the present study, direct correlations between human cortical bone mechanical and mineral properties and resorption localization by human osteoclasts were analysed. Resorbable and non-resorbable areas were characterized in terms of their mechanical and mineral properties. The mechanical properties with the Young's modulus and hardness were determined on the microscale by nanoindentation. The quantity and quality of minerals on the microscale were measured by RAMAN spectroscopy.

2. Material and methods

2.1. Bone sample preparation

Human cortical bones were collected from fresh cadavers by JC Auregan at Ecole de chirurgie du fer à Moulin, Lariboisière hospital (three male donors with a mean age of 72 years old), and immediately frozen at −20 °C. The age of the three bone male donors was respectively: donor 1: 69 years old; donor 2: 77 years old; donor 3: 71 years old. Every anatomical subject was free of systemic disease and did not take any medication before its inclusion in the study. However, given that no information about the BMD was available before the completion of the study, we collected the hip, distal radius and vertebras of each subject to ensure that none of these bones displayed any sign of osteoporosis. Nine plane-parallel samples (4 mm-long, 4-mm wide and 3-mm high) were cut in the diaphysis with a diamond saw (Secotom-15, Struers A/S, Ballerup, Denmark) transversally from the osteon direction (see Fig. 1a). The upper surface perpendicular to the osteon's direction was polished using a 1-μm diamond powder. Samples were then cleaned by ultrasonication in distilled water.

2.2. Human osteoclasts

Monocytes were purified from blood of healthy adult volunteer donors (Etablissement Français du Sang, Lyon Gerland, France) as previously described [19]. Mononuclear cells were isolated by density gradient centrifugation using Ficoll (Eurobio®), then centrifuged through a 50% Percoll gradient (GE Healthcare®). The light density fraction from the pellet was recovered and incubated for 10 min at room temperature in 3% human serum-PBS. Monocytes were purified from the light density fraction by immunomagnetic depletion (Dynal, Invitrogen®) using monoclonal antibodies (Immunotech, Beckman Coulter®) directed against CD19 (J3-119), CD3 (UCHT1), CD56 (C218) and CD235a (11E4B-7-6). Then, monocytes were cultured at 37 °C in 5% CO_2 using α-minimum essential medium (α-MEM, Life technologies®) supplemented with 2 mM L-glutamine (Gibco®), 100 U/mL penicillin (Gibco®), 100 μg/mL streptomycin (Gibco®), and 10% foetal bovine serum (FBS, Pan biotech Dutscher®). Monocytes were seeded in the presence of 50 ng/mL human M-CSF (PeproTech®) and 30 ng/mL human RANKL (PeproTech®). The medium and cytokines were changed after 3 days; M-CSF at 25 ng/mL and RANKL at 100 ng/mL. Osteoclasts were then detached from the plastic plates using Accutase (Sigma-Aldrich®) as previously described [20] and were seeded onto bone samples (50,000 cells/sample) with 25 ng/mL M-CSF and 100 ng/mL RANKL for 72 h (Fig. 1b). In the present study, osteoclasts from two blood donors were seeded on nine bone samples (see Table 1).

2.3. Nanoindentation

Prior to osteoclast seeding, nanoindentation tests were performed on the nine bone samples surrounded by a physiological saline solution at ambient temperature using a commercial nanoindenter (Agilent Nanoindenter G200, ScienTec, Les Ulis, France) (Fig. 1a). Fused silica was used to calibrate the Berkovich diamond tip contact surface. A grid of 81 measurement points per sample with a spacing of 150 μm

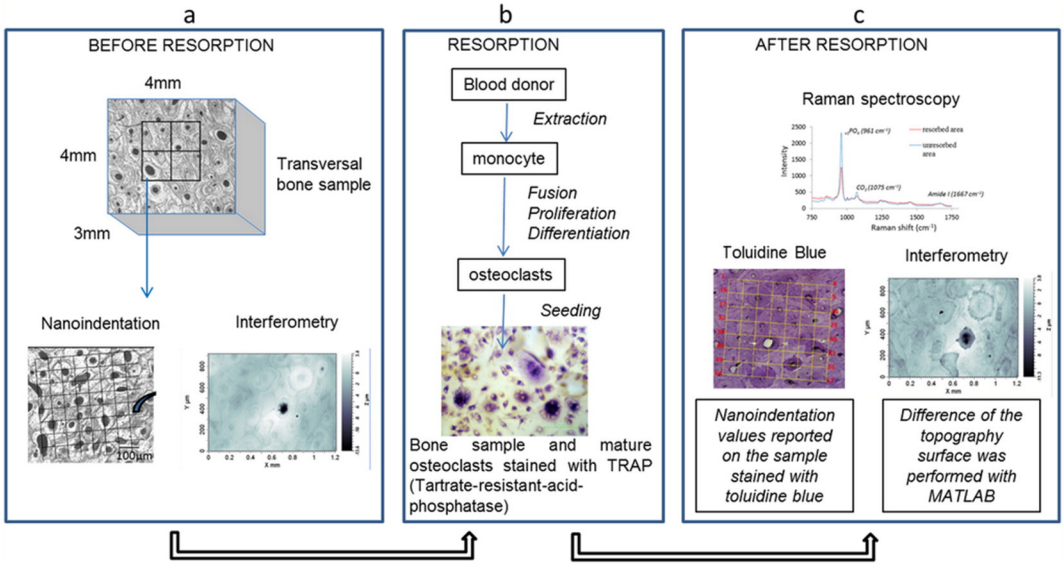

Fig. 1. Experimental design. The surface of each bone sample was characterized before seeding mature osteoclasts. First, nanoindentation and interferometer, respectively, provided local mechanical properties values and surface topography before resorption, respectively (panel a). In parallel, monocytes from human donors were extracted from peripheral blood and differentiated into osteoclasts. Then, osteoclasts were seeded on each sample in an optimal medium for osteoclast activity. After 72 h, osteoclasts were stained with TRAP, counted and removed from the bone surface (panel b). Next, the resorbed bone sample was stained by toluidine blue to determine the resorbed areas (intense violet). Analysis of the surface topography after resorption was carried out by interferometry on the same areas that were characterized before osteoclasts seeding. The variation of z (μm) at each point was measured and the mineral properties were characterized by Raman spectroscopy (panel c). (For interpretation of the references to colour in this figure legend, the reader is referred to the web version of this article.)

Table 1
Mechanical and mineral properties of each sample were analysed by nanoindentation and Raman spectroscopy. The Young's modulus and hardness values for each sample correspond to a mean value of 81 indents, and the mineral to matrix ratios, crystallinity and carbonate substitution rate correspond to a mean value of 30 points. Three human bone donors were used in this study.

Sample	Bone donor	Osteoclast donor	Young's modulus (GPa)	Hardness (GPa)	Mineral to matrix ratio ν_1PO_4 / Amide I	Mineral to matrix ratio ν_1PO_4 / CH_2	Crystallinity	Rate of carbonate substitution
1	1	1	21.7 ± 2.5	0.80 ± 0.13	15.60 ± 2.1	14.49 ± 0.9	0.0601 ± 0.0007	0.171 ± 0.006
2			22.1 ± 2.8	0.71 ± 0.14	14.68 ± 2.1	12.61 ± 1.9	0.0609 ± 0.0007	0.172 ± 0.006
3			21.7 ± 2.6	0.79 ± 0.14	17.18 ± 2.7	14.87 ± 1.2	0.0598 ± 0.001	0.172 ± 0.006
4	2	2	21.9 ± 2.3	0.79 ± 0.13	17.65 ± 1.5	15.37 ± 1.2	0.0604 ± 0.0009	0.162 ± 0.007
5			20.7 ± 2.6	0.73 ± 0.11	17.65 ± 1.1	15.87 ± 0.8	0.0611 ± 0.0009	0.162 ± 0.006
6			20.5 ± 2.4	0.62 ± 0.09	17.77 ± 2.4	15.92 ± 1.0	0.0605 ± 0.001	0.164 ± 0.008
7	3	2	20.3 ± 2.8	0.72 ± 0.11	17.43 ± 2.4	14.86 ± 1.5	0.0599 ± 0.001	0.190 ± 0.008
8			20.7 ± 2.1	0.73 ± 0.10	16.06 ± 2.2	14.31 ± 1.3	0.0593 ± 0.0007	0.172 ± 0.006
9			20.1 ± 2.0	0.69 ± 0.10	17.39 ± 1.6	14.96 ± 1.5	0.0599 ± 0.0009	0.169 ± 0.006
Mean			21.0	0.73	16.82	14.81	0.0602	0.1681
SD			±0.7	±0.06	±1.1	±0.9	±0.0006	±0.004

was performed. Then, nanoindentation points were at random locations inside the bone microstructure. A constant strain rate of 0.05 s^{-1} and a maximum depth of 2000 nm were imposed. The Continuous Stiffness Measurement (CSM) method allowed for the determination of the Young's modulus and the hardness as functions of the displacement into the surface. In the present study, Oliver and Pharr's method [21] was used with the assumptions for linear elastic isotropic material. The elastic properties of the diamond indenter were $\nu_i = 0.07$ and $E_i = 1131$ GPa. Moreover, bone was assumed to be isotropic, with a 0.3 Poisson ratio. The Young's modulus and hardness for each point were measured on the plateau between 600 and 1200 nm. The mean values of the Young's modulus and hardness for each sample are given in Table 1.

2.4. Raman spectroscopy

Raman spectroscopy (LabRAM HR 800, Horiba Jobin Yvon, Villeneuved'Ascq, France) was performed under wet conditions on the same sample surface as nanoindentation. This technique uses Raman scattering to obtain information on the composition of the material. A 785 nm laser was focused on the bone surface through a BX41 microscope (Olympus, Tokyo, Japan) with a 50× objective (NA = 0.75), resulting in a laser spot diameter of less than 2 μm. The system included a CCD camera (1024 × 256 pixels cooled by Peltier effect at −70 °C) to detect the Raman scattering and a grating of 1800 grooves/mm permitting to collect data with a spectral resolution less than 1 cm^{-1}. LabSpec 5 software (Horiba Jobin Yvon, Villeneuve d'Ascq, France) was used to de-spike the spectra and subtract the background. Before use, the instrument was calibrated to the 520.7 cm^{-1} Raman line of silicon. Thirty location points inside the bone microstructure were measured for each of the nine samples (15 points for resorbed areas, 15 points for unresorbed areas) corresponding to a total of 270 location points. For better reproducibility, one accumulation was used and five consecutive spectra were acquired in each location corresponding to 1350 spectra [22,23]. These five 45 s acquisitions were averaged at each location between 750 cm^{-1} and 1750 cm^{-1}. Accordingly, Raman peak ratios are usually used rather than peak intensities to detect differences in bone tissue composition. Then two intensity ratios were automatically calculated from the smoothed spectra (sliding average over three points corresponding to a range of 2 cm^{-1}). Three parameters were calculated from the smoothed spectrum: i) mineral-to-matrix ratio describing the mineral content compared to the collagen matrix was calculated in two ways: [1] ν_1PO_4 (961 cm^{-1}) / Amide I (1667 cm^{-1}) maximum intensities ratio and ν_1PO_4 (961 cm^{-1}) / CH_2 wag (1453 cm^{-1}) maximum intensities ratio; ii) the carbonate-to-phosphate ratio, which is the ratio between the CO_3 (1075 cm^{-1}) and the ν_1PO_4 (961 cm^{-1}), conveying the substitution rate; and iii) the crystallinity, which is the inverse of the full width at half-maximum of the ν_1PO_4 peak (961 cm^{-1}). The crystallinity value increases when the size of the mineral crystals increases [24] (Fig. 1c). As ν_1PO_4 and Amide I bands are orientation dependent [25] a large number of points was analysed to statistically compare resorbed and unresorbed osteons. The mean values of the mineral/matrix ratios, carbonate substitution rate and crystallinity for each sample are provided in Table 1.

2.5. Resorption analysis

After 72 h of osteoclast culture, osmotic lysis with water and sonication were used to remove cells. Then, the nine bone samples were stained in a toluidine blue solution. Toluidine blue intensely colours naked collagen fibres resulting from the resorption process. Resorbed areas were localized using an upright microscope under tangential light (Fig. 1c). The quantification of resorption was analysed using white light interferometry (Wyko NT, Veeco). Topography acquisition was performed before and after resorption in vertical scanning interferometry mode using Visio 32 software parameters: FOV 1×, 5× magnification, VSI optical speed 1×, backscan 20 μm, length 50 μm and 2.5 modulations. For each sample, four acquisitions were performed to cover 4 mm^2 in the centre of the sample surface (Fig. 1c). For each point of the sample, the variation depth Δz, corresponding to the height before resorption minus the height after resorption, and the percentage of the resorbed surface were calculated using a homemade Matlab routine.

2.6. Scanning electron microscopy

Scanning electron microscopy (SEM) acquisitions were taken in the backscattered electron mode to reflect the difference in mineralization with a Quanta 250 FEG microscope (FEI, Hillsboro, Oregon, USA) equipped with a GDA detector in environmental conditions. The microscope was operated at a voltage of 30 kV and hydrostatic pressure of 0.9 Torr (120 Pa) in the chamber. A magnification of 50× and a very slow scanning speed (30 μs per point) were used to obtain a contrasted image of 2.54 mm by 2.54 mm. Each image was resized to keep only the area of interest already analysed in the experiments of nanoindentation and Raman spectroscopy.

2.7. Statistical analysis

In the present study, a Kruskal-Wallis test was performed to analyze differences between the mechanical and mineral properties of values obtained on the three bone donors. Because no significant difference was observed between donors, resorption analysis was performed on the mean values of all samples. Differences between the resorbed and non-resorbed values were analysed using a Mann-Whitney test. A *P*-value of 0.05 was considered to be statistically significant.

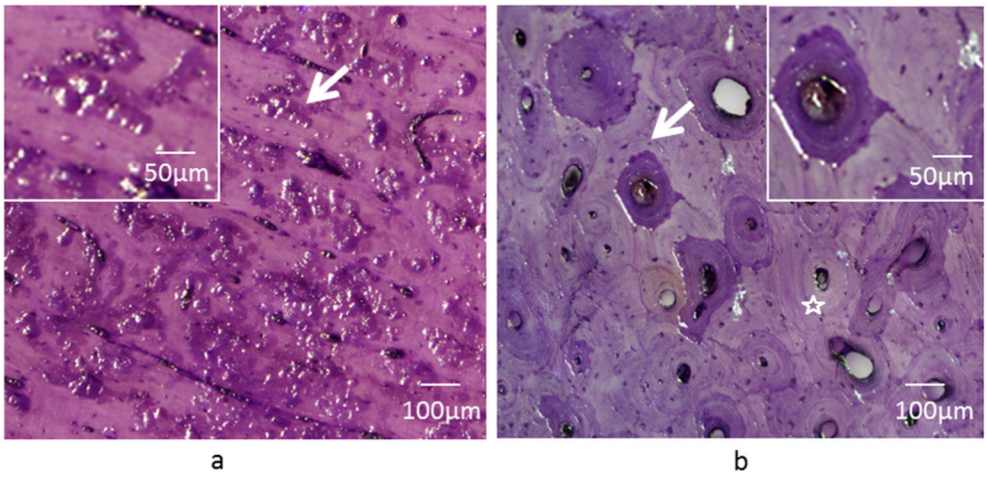

Fig. 2. Comparison of the resorption profile between bovine plexiform cortical bone and human haversian bone. Human osteoclasts were cultivated for 72 h on samples of bovine cortical bone (a) and human bone (b), in the presence of MCSF (macrophage colony-stimulated factor) and RANKL (receptor activator of NF-kB ligand). Cells removal and staining with toluidine blue (staining of naked collagen fibres) allows – using tangential light - to visualize resorption lacunae created by osteoclasts. (a) Observation of resorbed bovine plexiform bone reveals the random distribution of small lacunae called "pits" (arrow). (b) Resorption of human haversian cortical bone reveals the resorption of some osteons (white arrow) but not others (star). Enlarged area corresponds to a zoom of arrow zone. (For interpretation of the references to colour in this figure, the reader is referred to the web version of this article.)

3. Results

3.1. Resorption heterogeneity

In a first step, osteoclast resorption was studied in terms of localization within the cortical bone microstructure. For that purpose, classical identification of the resorption process was performed using toluidine blue staining, which colours collagen fibres, specifically the naked ones. To evaluate the impact of heterogeneity, we initially compared - under the same conditions - resorption by human osteoclasts of bovine plexiform cortical bone and human haversian cortical bone. 72 h after seeding the osteoclasts - derived from human peripheral blood - onto bovine cortical bone, in the presence of MCSF and RANKL, we observed random homogeneous resorption lacunae - or "pits" - within the matrix (Fig. 2a). By contrast, we found that resorption of human cortical bone by human osteoclasts was not homogeneous within the microstructure (Fig. 2b).

To better characterize the resorption profile of human cortical bone we first compare bone samples before and after resorption. Fig. 3a shows a typical cortical bone stained with toluidine blue before osteoclast seeding. Pale homogeneous coloration was observed. After 72 h of mature osteoclast culture, typical cortical bone surfaces from donor 1 (sample 1), donor 2 (sample 4), and donor 3 (sample 7) are shown in Fig. 3b, c, and d, respectively. For all samples, toluidine blue staining revealed a heterogeneous coloration within the microstructure. Osteoclasts resorbed some osteons (intense coloration and loss of matrix enhanced by tangential light; see the zoomed area in Fig. 3b, c and d, arrow) but not others (star), resulting in a very clear resorption contour corresponding to the cement line, while interstitial bone was not a preferential target of the osteoclasts (see the enlarged area in Fig. 3).

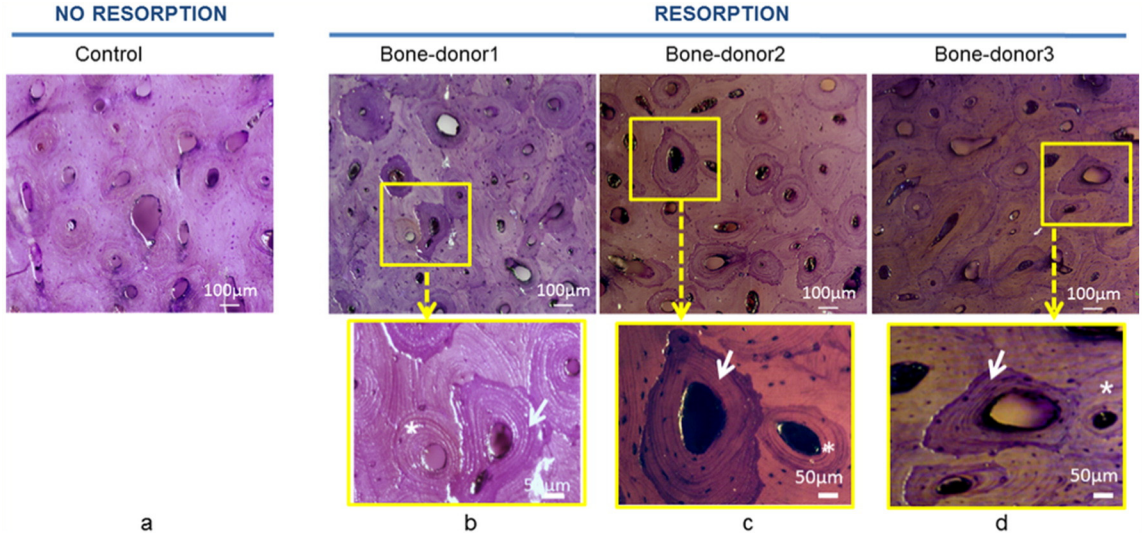

Fig. 3. Human osteoclasts resorb specific human cortical bone osteons. (a) Control: human cortical bone stained with toluidine blue observed using tangential light in the absence of osteoclast culture. Staining is weak and homogeneous within the osteons. (b) (c) (d) After culture of human osteoclasts for 72 h on human cortical bone samples, osteoclasts resorbed some osteons (arrow), but not neighbouring osteons (star). The same resorption profile was observed for all of the human bone donors: (b) donor 1 (c) donor 2 (d) donor 3 and for all of the samples studied. (For interpretation of the references to colour in this figure, the reader is referred to the web version of this article.)

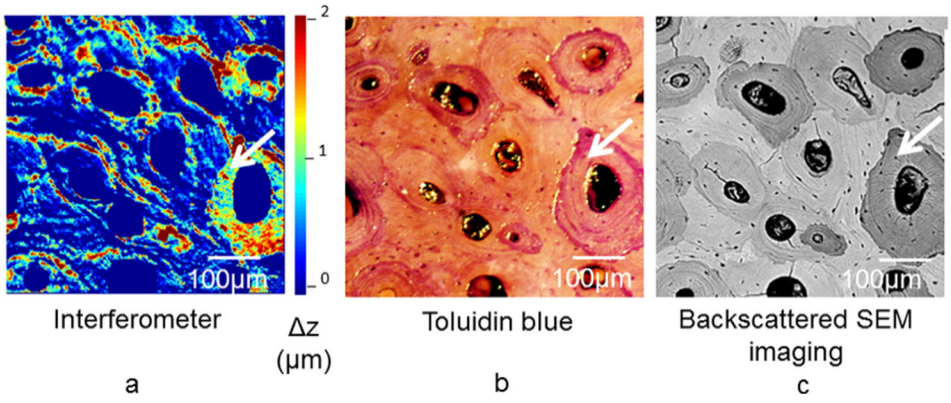

Fig. 4. Human osteoclasts specifically resorb osteons that have a poor mineral content. Comparison of the same human cortical bone area with different approaches showed a correlation between mineral content and localization and depth of resorption. (a) Interferometry measurements before and after resorption of the same bone area allow a representation after treatment to be obtained with MATLAB software with a z variation (Δz) before and after resorption (µm). The red colour scale indicates the resorption areas, whereas the blue colour scale indicates no resorption. (b) Toluidine blue staining of a sample after resorption, which colours collagen fibres, specifically the naked ones resulting from osteoclast activity. The intense toluidine blue staining is localized to the resorbed areas, and loss of matter is underlined with tangential light. (c) Backscattered SEM imaging of each samples before resorption reflected the degree of mineralization of each osteon. Mineralization differed from one osteon to another and from interstitial bone. The darkest osteons (arrow) correspond to youngest osteons with the lowest mineralization level. Therefore, the least mineralized areas (arrow) correspond to the most resorbed osteon (arrow). (For interpretation of the references to colour in this figure legend, the reader is referred to the web version of this article.)

3.2. Resorption quantification

To assess the resorption depth, a comparison of the topographic surface of each cortical bone sample before and after resorption was performed. Comparison of the same zone before and after resorption permitted to assess the loss of material (Δz in µm) at the osteon level. Quantitatively, the resorption depth was expressed as Δz (z before - z after resorption) in µm for each point of the same sample. A typical image of the resorption depth is shown in Fig. 4a. This topographic analysis confirmed a heterogeneous resorption process within the microstructure.

In a quantitative point of view, this comparison allowed to determine the values of the resorption depth as well as the fraction of the resorbed surface for each sample (Table 2). The mean values of the resorption depth and fraction of the resorbed surface obtained on all samples were 2.41 µm and 12.7%, respectively.

The resorption depth, obtained by interferometry, was compared with toluidine blue staining of the same area (Fig. 4b). The greater values of depth of resorption (Δz) correspond to more intense toluidine blue coloration after resorption. Then, toluidine blue staining image of all samples allows resorbed osteons and unresorbed osteons to be separated. In the same way, Fig. 4c shows the distribution of the mineral content obtained using SEM backscatter imaging. Because the darkest SEM grey level corresponds to the lowest mineral content, resorbed osteons were associated with a lower mineral content usually linked with the mechanical properties [26]. As a result, the mechanical and mineral contents play a significant role in osteoclast resorption. However, a decrease in the mineral content does not necessarily involve a modification of the mineral quality.

Table 2
Topographic analysis of the human cortical bone resorption profile. Each cortical bone sample was analysed by interferometry before and after resorption. Comparison of the topographic data allowed the quantification of resorbed areas delta z (µm) and resorbed surface percentage.

Sample	Mean value of resorbed osteons deltaZ (µm)	Resorbed surface percentage
1	2.63	13.4
2	1.77	12.4
3	3.38	11.1
4	2.90	13.6
5	2.47	13.0
6	2.06	12.3
7	2.19	11.7
8	1.78	14.3
9	2.59	12.2
Mean values	2.41 ± 0.52	12.7 ± 0.99

3.3. Mechanical and mineral quality properties

We compared the mechanical and mineral properties of resorbed *versus* unresorbed osteons and aimed to define a specific signature of the areas targeted by osteoclasts. The mechanical values measured before resorption using the nanoindentation technique are given in Table 3 for both types of osteon. The mean values of Young's modulus (E) and hardness (H) for future resorbed osteons were significantly lower (E = 19.7 GPa and H = 0.68 GPa, respectively) compared to future unresorbed osteons (E = 22.9 GPa and H = 0.80 GPa, respectively).

Then, the mineral characteristics of resorbed and unresorbed osteons were measured using Raman spectroscopy. The usual parameters analysed in bone Raman spectroscopy, such as the mineral-to-matrix ratios, carbonate-to-phosphate ratio and crystallinity for both types of osteons, were measured and are shown in Table 4. The mineral to matrix ratios and the crystallinity for resorbed osteons were significantly lower than for unresorbed osteons (resorbed osteons, respectively, 16.2 and 0.0596 *vs* unresorbed osteons 17.6 and 0.0614). The carbonate substitution rate of resorbed osteons was significantly higher than that of unresorbed osteons (resorbed osteons 0.172 *vs* unresorbed osteons 0.163). Therefore, osteoclasts preferentially target the lowest mineral content areas with specific mineral characteristics, such as small crystals with a lower crystal quality and a higher carbonate substitution rate.

4. Discussion

The goal of our study was to better understand the links between the mechanical properties of the human cortical bone surface and human osteoclast mediated resorption. To date, the vast majority of *in vitro* studies on osteoclast mediated bone degradation have been performed using cortical bovine bone, dentin or biomaterials, which provide relatively homogeneous surfaces [27–29]. In contrast, the human haversian cortical bone microstructure is composed of osteonal units [30] derived from the remodeling process, implying osteoclast activity. The elastic modulus and mineral content were shown to be almost constant inside the same osteon, but variable across osteons [16, 31 and 32]. The hardest tissues inside the microstructure are interstitial tissues that are mainly composed of the remains of aging osteons [33].

Table 3
Human osteoclasts resorb target areas with the lowest mechanical properties. Values of nanoindentation measurements obtained before resorption were superimposed on the toluidine blue resorption image obtained after resorption. Thus, each measurement was determined as a future resorbed area or unresorbed area. Osteoclasts preferentially resorbed areas with the lowest Young's modulus and hardness values. Statistics: (Mann-Whitney *U* test).

Nanoindentation	Resorbed osteons	Unresorbed osteons	*P* value
Young's modulus (GPa)	19.7 ± 0.7	22.9 ± 1.3	$9.49 \cdot 10^{-6}$
Hardness (GPa)	0.68 ± 0.05	0.8 ± 0.07	$9.45 \cdot 10^{-5}$

We raised the question of whether osteoclasts could sense their environment, such as the heterogeneous microstructure, and preferentially resorb bone surfaces with characteristic mechanical and mineral properties.

Several studies have shown that *in vitro* osteoclast-mediated bone degradation implies that there are very dynamic cell behaviours linked to the actin dynamic [34]. Indeed, osteoclasts adhere to the extracellular matrix through integrins that are associated with a dense network of actin and proteins that form podosomes [35]. On mineralized surfaces, they form a sealing zone that is composed of an interlinked network of podosomes, which delimits the degradation lacuna into which osteoclasts secrete acid and proteolytic enzymes [36]. Labernardie et al. showed that podosomes from macrophages exert pushing forces on their substrates [37] and that they possess mechanosensing properties, *i.e.*, the capacity to sense substrate rigidity. Moreover, B. Geiger's group provided evidence that sealing zones can sense the heterogeneity of adhesion surfaces [38,39]. Through these actin dynamic structures, osteoclasts are mechanosensitive cells that are able to sense substrate rigidity. In this study, we studied, in detail, human monocyte-derived osteoclast activity on human haversian cortical bone, as a function of its structural, mechanical and chemical heterogeneities. We provide evidence that human cortical bone resorption, in contrast to bovine cortical bone, dentin or synthetic biomaterials, is not a random process. Indeed, we observed that the osteoclasts that are seeded homogeneously on the surface of human cortical bone resorbed preferentially within osteons, whereas interstitial bone was untouched. Human cortical bone sample topographic analysis defined a mean value of the resorption depth of 2.4 μm in our culture conditions. To our knowledge, no other study has analysed the depth of human osteoclast resorption on human bone *in vitro*. However, the order of values measured is consistent with the data found in the literature [10,40], even if the *in vitro* culture conditions were variable. For instance, in 2006, Varghese et al. reported a pit depth of 1.42 μm for mouse osteoclasts that were cultured for 48 h on dentin [29].

Moreover, heterogeneity also exists within osteons because osteons targeted by human osteoclasts had the weakest mechanical properties in terms of the Young's modulus/hardness. The average Young's modulus and hardness values before resorption for the resorbed areas were 19.7 GPa and 0.68 GPa, respectively, compared to the unresorbed areas, with 22.9 GPa and 0.80 GPa. These results indicate that osteoclasts can sense bone surface mechanical heterogeneity to degrade it. In a previous study, we showed that on homogeneous surfaces, such as glass; synthetic mineralized surfaces; dentin; or cortical bone, murine osteoclasts alternate between migration phases with a loose actin network and resorption phases with the formation of an actin containing sealing zone [35,41,and 42]. We can now determine that on heterogeneous human cortical bone surfaces, osteoclasts resorb specific areas, mostly within osteons. Then, osteons are completely resorbed along the main axis of the haversian structure. This indicates that once located within osteons, osteoclasts are constrained within a physical barrier. This is in agreement with the results published by Anderegg et al., showing that the sealing zone organization and dynamics of murine osteoclasts seeded on micro-patterned glass substrates strictly depend on the continuity of substrate adhesiveness [43].

Furthermore, our study provides evidence that osteons targeted by osteoclasts had a lower mineralization content compared to unresorbed osteons and interstitial bone. This result is in agreement with the weak mechanical properties of these areas because a positive correlation exists between the mineral content and mechanical properties [26]. Different studies have described the effect of mineral density on osteoclast activity [11,44]. The only study that used a human cortical bone substrate concluded that chick osteoclasts resorbed homogeneous density mineral areas in 60% of the cases. In addition Jones et al. showed that for elephant teeth, the rate of resorption was inversely proportional to the mineral density [44], whereas Taylor et al. showed the same relationship for the rate of rabbit osteoclast activity on biomaterials [45].

In this study, we highlighted that osteons targeted by osteoclasts are characterized by smaller hydroxyapatite crystals and a higher carbonate substitution rate compared to non-resorbed areas in human cortical bone. In bone tissue engineering, the interaction of osteoclasts with biomaterials with different compositions, crystallinities, grain sizes and surface bioactivities in regard to the degradation activity has been investigated [9]. The resorbability of different bone substitutes by human osteoclasts is not equivalent [46]. Indeed, the composition of synthetic material is a major parameter that inhibits or enhances osteoclast-mediated resorption. In particular, the crystallinity, grain size [47,48] and roughness affect osteoclast activity [38]. Concerning the rate of carbonate substitution, it is known that substitutions within the hydroxyapatite crystals, such as carbonate, provokes a stoichiometric variation, resulting in a loss of mineral quality [49]. Another study on ceramics reported that the resorption increased with the carbonate substitution content [50]. Therefore, our results emphasize the impact of the heterogeneity of the human bone microstructure in terms of the mechanical and mineral properties on osteoclast activity. In the same way, Dong et al. [51] observed that the bone resorption activities of osteoclasts were positively correlated with the *in situ* concentration of advanced glycation end products (AGEs). Then, it will be interesting to analyze AGEs accumulation in future work.

Our results showed clearly a strong impact of microstructure, osteoclasts resorbing preferentially osteons with mechanically softer properties. This result raises the question; how older tissues are resorbed *in vivo*? Actually, *in vivo* bone remodeling process aims to maintain bone mechanical properties and mineral homeostasis. It seems that two

Table 4
Osteoclasts preferentially resorbed areas that had the lowest mineral content, contained small crystals, and whose maturation was the most advanced. The bone mineral characteristics were obtained with RAMAN microspectroscopy. The mineral/matrix ratios reflect the rates of mineralization, crystallinity reflects the size of the crystal, and the rate of carbonate substitution reflects the mineral maturation. Each value corresponds to a mean value of 9 samples, with 15 measurements per sample. Osteoclasts preferentially resorbed areas with the lowest levels of mineralization, the smallest crystals and areas with the highest rates of carbonate substitution. Statistics: (Mann-Whitney *U* test).

Raman spectroscopy	Resorbed osteons	Unresorbed osteons	*P* value
Mineral to matrix ratios			
ν_1PO_4 (961 cm^{-1}) / Amide I (1667 cm^{-1})	16.2 ± 1.4	17.6 ± 0.8	0.010
ν_1PO_4 (961 cm^{-1}) / CH_2 (1450 cm^{-1})	13.9 ± 1.2	15.7 ± 0.8	0.004
Crystallinity			
the inverse of the full width at half maximum of the ν_1PO_4 peak (961 cm^{-1})	0.0596 ± 0.001	0.0614 ± 0.005	$1.94 \cdot 10^{-5}$
Carbonate substitution rate			
CO_3 (1075 cm^{-1}) / ν_1PO_4 (961 cm^{-1})	0.172 ± 0.005	0.163 ± 0.004	0.004

kinds of bone remodeling exist: one that is "stochastic" and a second that is targeted to areas that require repair such as microcracks created by repetitive cycles of mechanical loading [52–55]. Microcracks accumulation is more important in older tissue as it increased with the number of cycles. Targeted remodeling process is based on a strong association between microdamage and osteocyte apoptosis, which is an important factor in initiating new remodeling sites [56]. Because, no mechanical stimulation was applied on bone sample during osteoclast culture and osteocytes were dead, fatigue microcrack accumulation removal cannot be observed in our experiments. In this context, osteoclast resorption measured in the present study corresponds to "stochastic" remodeling which serves functions other than microdamage removal such as metabolic function. Moreover, results obtained in this study suggest that "stochastic" remodeling does not operate truly in a random manner.

The results obtained in the present *in vitro* study present similarities with recent results obtained on bone pathologies, such as osteogenesis imperfecta. In fact, this bone pathology is characterized by large resorption cavities, leading to a weak fracture resistance [57]. These large cavities were also associated with local altered mechanical properties and the crystal quality compared to the bones of healthy children [58]. In particular, osteogenesis imperfecta bones are composed of small crystals, which in regard to our study, were associated with an increase in bone resorption. Furthermore, Gourion-Arsiquaud et al. [59] have shown a reduction of the heterogeneity of mineral-to-matrix and carbonate-to-phosphate ratios and more variable crystallinity in fracture cases compared with fracture-free controls. It will be interesting to compare osteoclast activity between these two groups. The crystal quality and mechanical properties at the local scale are then key parameters for osteoclast behaviour, for both *in vitro* and clinical studies.

This study demonstrates that the substrate microstructure influences osteoclast activity. The resorption profile on the human haversian cortical bone microstructure revealed a correlation between the resorbed areas and the mechanical and mineral properties. The resorbed areas matched clearly with the osteon geometry. Osteons targeted by osteoclasts are weaker in terms of their mechanical properties (Young's modulus and Hardness) and mineral quantity and quality (a small crystallinity value and high carbonate substitution rate) than non-resorbable areas. Future *in vitro* resorption studies must take into account the influence of substrate properties on the osteoclast activity. It would also be interesting to study the direct impact of variations in the bone properties in bone diseases or tissue engineering [60] on osteoclast activity.

Acknowledgements

This work has been supported through grants from ANR-10-EQPX-06-01 IVTV, and ANR-11-BS09-036-01 OMBIOS. We thank the French Establishment of blood (EFS) for the blood sample as well as "Ecole de chirurgie du fer à Moulin Lariboisière" for the access to the human bone samples.

References

[1] E.F. Eriksen, G.Z. Eghbali-Fatourechi, S. Khosla, Remodeling and vascular spaces in bone, J. Bone Miner. Res. 22 (2007) 1–6, http://dx.doi.org/10.1080/14041040701482935.
[2] M. Zaidi, Skeletal remodeling in health and disease, Nat. Med. 13 (2007) 791–801, http://dx.doi.org/10.1038/nm1593.
[3] Y. Bala, D. Farlay, G. Boivin, Bone mineralization: from tissue to crystal in normal and pathological contexts, Osteoporos. Int. 24 (2013) 2153–2166, http://dx.doi.org/10.1007/s00198-012-2228-y.
[4] W.J. Boyle, W.S. Simonet, D.L. Lacey, Osteoclast differentiation and activation, Nature 423 (2003) 337–342, http://dx.doi.org/10.1038/nature01658.
[5] S.L. Teitelbaum, Bone resorption by osteoclasts, Science 289 (2000) 1504–1508.
[6] M.T. Drake, B.L. Clarke, E.M. Lewiecki, The pathophysiology and treatment of osteoporosis, Clin. Ther. (2015), http://dx.doi.org/10.1016/j.clinthera.2015.06.006.
[7] M.S. Davis, B.L. Kovacic, J.C. Marini, A.J. Shih, K.M. Kozloff, Increased susceptibility to microdamage in Brtl/+ mouse model for osteogenesis imperfecta, Bone 50 (2012) 784–791, http://dx.doi.org/10.1016/j.bone.2011.12.007.
[8] B.F. Boyce, Advances in osteoclast biology reveal potential new drug targets and new roles for osteoclasts, J. Bone Miner. Res. 28 (2013) 711–722, http://dx.doi.org/10.1002/jbmr.1885.
[9] R. Detsch, A.R. Boccaccini, The role of osteoclasts in bone tissue engineering, J. Tissue Eng. Regen. Med. (2014), http://dx.doi.org/10.1002/term.1851.
[10] M. Rumpler, et al., Osteoclasts on bone and dentin in vitro: mechanism of trail formation and comparison of resorption behavior, Calcif. Tissue Int. 93 (2013) 526–539, http://dx.doi.org/10.1007/s00223-013-9786-7.
[11] M. Nakamura, T. Hentunen, J. Salonen, A. Nagai, K. Yamashita, Characterization of bone mineral-resembling biomaterials for optimizing human osteoclast differentiation and resorption, J. Biomed. Mater. Res. A 101 (2013) 3141–3151, http://dx.doi.org/10.1002/jbm.a.34621.
[12] G.W. Marshall Jr., Dentin: microstructure and characterization, Quintessence Int. 24 (1993) 606–617.
[13] J.Y. Rho, L. Kuhn-Spearing, P. Zioupos, Mechanical properties and the hierarchical structure of bone, Med. Eng. Phys. 20 (1998) 92–102.
[14] D.B. Burr, M.B. Schaffler, R.G. Frederickson, Composition of the cement line and its possible mechanical role as a local interface in human compact bone, J. Biomech. 21 (1988) 939–945.
[15] R. Lakes, S. Saha, Cement line motion in bone, Science 204 (1979) 501–503.
[16] T. Hoc, et al., Effect of microstructure on the mechanical properties of Haversian cortical bone, Bone 38 (2006) 466–474, http://dx.doi.org/10.1016/j.bone.2005.09.017.
[17] M.L. Hillier, L.S. Bell, Differentiating human bone from animal bone: a review of histological methods, J. Forensic Sci. 52 (2007) 249–263, http://dx.doi.org/10.1111/j.1556-4029.2006.00368.x.
[18] S.A. Reid, Effect of mineral content of human bone on in vitro resorption, Anat. Embryol. 174 (1986) 225–234.
[19] A. Rivollier, et al., Immature dendritic cell transdifferentiation into osteoclasts: a novel pathway sustained by the rheumatoid arthritis microenvironment, Blood 104 (2004) 4029–4037, http://dx.doi.org/10.1182/blood-2004-01-0041.
[20] U. Harre, D. Georgess, H. Bang, A. Bozec, R. Axmann, E. Ossipova, P. Jakobsson, W. Baum, F. Nimmerjahn, E. Szarka, G. Sarmay, G. Krumbholz, E. Neumann, R. Toes, H. Scherer, A. Catrina, L. Klareskog, P. Jurdic, G. Schett, Induction of osteoclastogenesis and bone loss by human autoantibodies against citrullinated vimentin, J. Clin. Invest. 122 (2012) 1791–1802, http://dx.doi.org/10.1172/JCI60975.
[21] W. Oliver, G.M. Pharr, An improved technique for determining hardness and elastic modulus using load and displacement sensing indentation experiments, J. Mater. Res. 7 (1992) 1564–1583.
[22] M. Hammond, A. Berman, R. Pacheco-Costa, H. Davis, L. Plotkin, J. Wallace, Removing or truncating connexin 43 in murine osteocytes alters cortical geometry, nanoscale morphology, and tissue mechanics in the tibia, Bone 88 (2016) 85–91, http://dx.doi.org/10.1016/j.bone.2016.04.021.
[23] L. Imbert, J.C. Auregan, K. Pernelle, T. Hoc, Mechanical and mineral properties of osteogenesis imperfecta human bones at the tissue level, Bone 65 (2014) 18–24, http://dx.doi.org/10.1016/j.bone.2014.04.030.
[24] J.S. Yerramshetty, C. Lind, O. Akkus, The compositional and physicochemical homogeneity of male femoral cortex increases after the sixth decade, Bone 39 (2006) 1236–1243, http://dx.doi.org/10.1016/j.bone.2006.06.002.
[25] M. Kazanci, P. Roschger, E.P. Paschalis, K. Klaushofer, P. Fratzl, Bone osteonal tissues by Raman spectral mapping: Orientation–composition, J. Struct. Biol. 156 (2006) 489–496, http://dx.doi.org/10.1016/j.jsb.2006.06.011.
[26] T.T. Huang, L.H. He, M.A. Darendeliler, M.V. Swain, Correlation of mineral density and elastic modulus of natural enamel white spot lesions using X-ray microtomography and nanoindentation, Acta Biomater. 6 (2010) 4553–4559, http://dx.doi.org/10.1016/j.actbio.2010.06.028.
[27] J. Aerssens, S. Boonen, G. Lowet, J. Dequeker, Interspecies differences in bone composition, density, and quality: potential implications for in vivo bone research, Endocrinology 139 (1998) 663–670, http://dx.doi.org/10.1210/endo.139.2.5751.
[28] T. Hefti, M. Frischherz, N.D. Spencer, H. Hall, F. Schlottig, A comparison of osteoclast resorption pits on bone with titanium and zirconia surfaces, Biomaterials 31 (2010) 7321–7331, http://dx.doi.org/10.1016/j.biomaterials.2010.06.009.
[29] B.J. Varghese, K. Aoki, H. Shimokawa, K. Ohya, Y. Takagi, Bovine deciduous dentine is more susceptible to osteoclastic resorption than permanent dentine: results of quantitative analyses, J. Bone Miner. Metab. 24 (2006) 248–254, http://dx.doi.org/10.1007/s00774-005-0679-3.
[30] M.L. Brandi, Microarchitecture, the key to bone quality, Rheumatology (Oxford) 48 (Suppl. 4) (2009) iv3–iv8, http://dx.doi.org/10.1093/rheumatology/kep273.
[31] P. Roschger, H. Plenk Jr., K. Klaushofer, J. Eschberger, A new scanning electron microscopy approach to the quantification of bone mineral distribution: backscattered electron image grey-levels correlated to calcium K alpha-line intensities, Scanning Microsc. 9 (1995) 75–86 (discussion 86–78).
[32] O. Akkus, F. Adar, M.B. Schaffler, Age-related changes in physicochemical properties of mineral crystals are related to impaired mechanical function of cortical bone, Bone 34 (2004) 443–453, http://dx.doi.org/10.1016/j.bone.2003.11.003.
[33] J.Y. Rho, P. Zioupos, J.D. Currey, G.M. Pharr, Microstructural elasticity and regional heterogeneity in human femoral bone of various ages examined by nano-indentation, J. Biomech. 35 (2002) 189–198.
[34] P. Jurdic, F. Saltel, A. Chabadel, O. Destaing, Podosome and sealing zone: specificity of the osteoclast model, Eur. J. Cell Biol. 85 (2006) 195–202, http://dx.doi.org/10.1016/j.ejcb.2005.09.008.

[35] D. Georgess, I. Machuca-Gayet, A. Blangy, P. Jurdic, Podosome organization drives osteoclast-mediated bone resorption, Cell Adhes. Migr. 8 (2014) 191–204.
[36] S. Yovich, et al., Evidence that failure of osteoid bone matrix resorption is caused by perturbation of osteoclast polarization, Histochem. J. 30 (1998) 267–273.
[37] A. Labernadie, et al., Protrusion force microscopy reveals oscillatory force generation and mechanosensing activity of human macrophage podosomes, Nat. Commun. 5 (2014) 5343, http://dx.doi.org/10.1038/ncomms6343.
[38] D. Geblinger, L. Addadi, B. Geiger, Nano-topography sensing by osteoclasts, J. Cell Sci. 123 (2010) 1503–1510, http://dx.doi.org/10.1242/jcs.060954.
[39] D. Geblinger, C. Zink, N.D. Spencer, L. Addadi, B. Geiger, Effects of surface microtopography on the assembly of the osteoclast resorption apparatus, J. R. Soc. Interface 9 (2012) 1599–1608, http://dx.doi.org/10.1098/rsif.2011.0659.
[40] G. Mabilleau, F. Pascaretti-Grizon, M.F. Basle, D. Chappard, Depth and volume of resorption induced by osteoclasts generated in the presence of RANKL, TNF-alpha/IL-1 or LIGHT, Cytokine 57 (2012) 294–299, http://dx.doi.org/10.1016/j.cyto.2011.11.014.
[41] P. Jurdic, F. Saltel, A. Chabadel, O. Destaing, Podosome and sealing zone: specificity of the osteoclast model, Eur. J. Cell Biol. 85 (2006) 195–202, http://dx.doi.org/10.1016/j.ejcb.2005.09.008.
[42] S. Hu, et al., Podosome rings generate forces that drive saltatory osteoclast migration, Mol. Biol. Cell 22 (2011) 3120–3126, http://dx.doi.org/10.1091/mbc.E11-01-0086.
[43] F. Anderegg, et al., Substrate adhesion regulates sealing zone architecture and dynamics in cultured osteoclasts, PLoS One 6 (2011), e28583, http://dx.doi.org/10.1371/journal.pone.0028583.
[44] S.J. Jones, M. Arora, A. Boyde, The rate of osteoclastic destruction of calcified tissues is inversely proportional to mineral density, Calcif. Tissue Int. 56 (1995) 554–558.
[45] D. Taylor, J.G. Hazenberg, T.C. Lee, Living with cracks: damage and repair in human bone, Nat. Mater. 6 (2007) 263–268, http://dx.doi.org/10.1038/nmat1866.
[46] A.F. Schilling, et al., Resorbability of bone substitute biomaterials by human osteoclasts, Biomaterials 25 (2004) 3963–3972, http://dx.doi.org/10.1016/j.biomaterials.2003.10.079.
[47] F. Despang, et al., Synthesis and physicochemical, in vitro and in vivo evaluation of an anisotropic, nanocrystalline hydroxyapatite bisque scaffold with parallel-aligned pores mimicking the microstructure of cortical bone, J. Tissue Eng. Regen. Med. (2013), http://dx.doi.org/10.1002/term.1729.
[48] R. Detsch, et al., The resorption of nanocrystalline calcium phosphates by osteoclast-like cells, Acta Biomater. 6 (2010) 3223–3233, http://dx.doi.org/10.1016/j.actbio.2010.03.003.
[49] O.O. Aruwajoye, H.K. Kim, P.B. Aswath, Bone apatite composition of necrotic trabecular bone in the femoral head of immature piglets, Calcif. Tissue Int. 96 (2015) 324–334, http://dx.doi.org/10.1007/s00223-015-9959-7.
[50] G. Spence, N. Patel, R. Brooks, W. Bonfield, N. Rushton, Osteoclastogenesis on hydroxyapatite ceramics: the effect of carbonate substitution, J. Biomed. Mater. Res. A 92 (2010) 1292–1300, http://dx.doi.org/10.1002/jbm.a.32373.
[51] X.N. Dong, A. Qin, J. Xu, X. Wang, In situ accumulation of advanced glycation endproducts (AGEs) in bone matrix and its correlation with osteoclastic bone resorption, Bone 49 (2011) 174–183, http://dx.doi.org/10.1016/j.bone.2011.04.009.
[52] D.B. Burr, Targeted and nontargeted remodeling, Bone 30 (2002) 2–4, http://dx.doi.org/10.1016/S8756-3282(01)00619-6.
[53] R. Martin, Is all cortical bone remodeling initiated by microdamage? Bone 30 (2002) 8–13, http://dx.doi.org/10.1016/S8756-3282(01)00620-2.
[54] A.M. Parfitt, G.R. Mundy, G.D. Roodman, D.E. Hughes, B.F. Boyce, A new model of the regulation of bone resorption, with particular reference to the effects of bisphosphonates, J. Bone Miner. Res. 11 (1996) 150–159, http://dx.doi.org/10.1002/jbmr.5650110203.
[55] B. Clarke, Normal bone anatomy and physiology, Clin. J. Am. Soc. Nephrol. 3 (2008) S131–S139, http://dx.doi.org/10.2215/CJN.04151206.
[56] O. Verborgt, G.J. Gibson, M.B. Schaffler, Loss of osteocyte integrity in association with microdamage and bone remodeling after fatigue in vivo, J. Bone Miner. Res. 15 (2000) 60–67, http://dx.doi.org/10.1359/jbmr.2000.15.1.60.
[57] F.S. van Dijk, et al., Osteogenesis imperfecta: a review with clinical examples, Mol. Syndromol. 2 (2011) 1–20, http://dx.doi.org/10.1159/000332228.
[58] L. Imbert, J.C. Auregan, K. Pernelle, T. Hoc, Microstructure and compressive mechanical properties of cortical bone in children with osteogenesis imperfecta treated with bisphosphonates compared with healthy children, J. Mech. Behav. Biomed. Mater. 46 (2015) 261–270, http://dx.doi.org/10.1016/j.jmbbm.2014.12.020.
[59] S. Gourion-Arsiquaud, et al., Fourier transform infrared imaging of femoral neck bone: reduced heterogeneity of mineral-to-matrix and carbonate-to-phosphate and more variable crystallinity in treatment-naive fracture cases compared with fracture-free controls, J. Bone Miner. Res. Off. J. Am. Soc. Bone Miner. Res. 28 (2013) 150–161, http://dx.doi.org/10.1002/jbmr.1724.
[60] E.S. Place, N.D. Evans, M.M. Stevens, Complexity in biomaterials for tissue engineering, Nat. Mater. 8 (2009) 457–470, http://dx.doi.org/10.1038/nmat2441.